

## X-RAY CLUSTER ASSOCIATED WITH THE Z=1.063 CSS QUASAR 3C 186: THE JET IS NOT FRUSTRATED.

ANETA SIEMIGINOWSKA<sup>1</sup>, C. C. CHEUNG<sup>2,3</sup>, STEPHANIE LAMASSA<sup>1</sup>, D. J. BURKE<sup>1</sup>, THOMAS L.  
ALDCROFT<sup>1</sup>, JILL BECHTOLD<sup>4</sup>, MARTIN ELVIS<sup>1</sup>, D.M. WORRALL<sup>5</sup>

*Draft version November 15, 2018*

### ABSTRACT

We report the *Chandra* discovery of an X-ray cluster at redshift  $z = 1.063$  associated with the Compact Steep Spectrum radio loud quasar 3C 186 (Q0740+380). Diffuse X-ray emission is detected out to  $\sim 120$  kpc from the quasar and contains  $741 \pm 40$  net counts. The X-ray spectrum of the extended emission shows strong Fe-line emission (EW=412eV) at the quasar redshift and confirms the thermal nature of this diffuse component. We measure a cluster temperature of  $5.2_{-0.9}^{+1.2}$  keV and an X-ray luminosity  $L_{(0.5-2\text{keV})} \sim 6 \times 10^{44}$  erg sec $^{-1}$ , which are in agreement with the luminosity-temperature relation for high-redshift clusters. This is the first detection of a bright X-ray cluster around a luminous ( $L_{\text{bol}} \sim 10^{47}$  erg sec $^{-1}$ ) CSS quasar at high redshift and only the fifth  $z > 1$  X-ray cluster detected. We find that the CSS radio source is highly overpressured with respect to the thermal cluster medium by about 3 orders of magnitude. This provides direct observational evidence that the radio source is not thermally confined as posited in the “frustrated” scenario for CSS sources. Instead, it appears that the radio source may be young and we are observing it at an early stage of its evolution. In that case the radio source could supply the energy into the cluster and potentially prevent its cooling.

*Subject headings:* quasars: individual (3C 186) - X-rays: galaxies: clusters

### 1. INTRODUCTION

Powerful radio sources, that are compact on galaxy scales, the Giga-Hertz Peaked Spectrum (GPS) and Compact Steep Spectrum (CSS) sources, comprise a significant fraction of the bright radio source population (10-20%, O’Dea 1998). They are strong candidates for being the progenitors of large-scale radio sources (e.g. Fanti et al. 1995, O’Dea & Baum 1997, O’Dea 1998), but this connection has not been firmly established. Their radio morphologies show compact emission on arcsec (VLA resolution) scales while on milliarcsec scales (VLBI) the sources look remarkably like scaled down large radio galaxies, where the entire radio structure (1-10 kpc) is enclosed within the host galaxy. Since the first GPS samples have been constructed there has been a clear controversy regarding their nature (see O’Dea 1998 and references therein). In the *evolution* model the source size and the characteristic spectral break at GHz radio frequencies could be an indication of young age, while in the other model the radio jet could be *frustrated* by a dense confining medium. Recent observations (e.g. measured expansion timescales of  $< 1000$  years, Owsianik et al. 1998, Polatidis & Conway 2003) give more weight to the *evolution* model (Readhead et al. 1996, Snellen et al. 2000, Alexander 2000), although there has been no definite observational evidence to rule out either of the models and both interpretations are still viable.

Here, we report the *Chandra* discovery of extended X-ray emission associated with the compact steep spectrum (CSS) quasar, 3C 186 (Q0740+380,  $z=1.063$ ). The

*Chandra* spectrum of the diffuse emission contains  $741 \pm 40$  counts and a strong (EW $\sim 412$ eV) iron emission line at the quasar redshift characteristic of thermal emission. This is the first observation of thermal emission associated with a CSS quasar at high redshift and gives us a rare opportunity to study interactions between an expanding CSS radio source and the cluster medium. As we show in Section 6.2 that the pressure of the hot cluster gas is too low, by 2-3 orders of magnitudes, to confine the radio source. This is direct observational evidence that the radio source is not thermally confined, and so instead is presumably young so that we are observing it at an early stage of its evolution.

Over the last decade attempts have been made to find X-ray clusters associated with radio-loud sources at high redshift (e.g. O’Dea 2000, Siemiginowska et al 2003 for studies related to GPS and CSS). If the clusters are found around large number of radio-loud sources then this could be used to place constraints on structure-formations models at large redshift. Bremer, Fabian & Crawford (1997) describe the model for an onset of a powerful radio source in the center of a cooling flow cluster. Such a cluster could also confine a compact radio source. The limited capabilities of the available X-ray telescopes allowed only for a few detections of extended X-ray emission around radio sources at redshifts  $z > 0.3$  (Hardcastle & Worrall 1999, Crawford & Fabian 2003, Worrall et al. 2001). High dynamic range observations are required to detect faint diffuse emission in the vicinity of a bright powerful source. The *Chandra* X-ray Observatory can resolve spatially distinct X-ray emission components in the vicinity of a strong X-ray source with  $\sim 1$  arcsec resolution and a high dy-

<sup>1</sup> Harvard-Smithsonian Center for Astrophysics, 60 Garden St., Cambridge, MA 02138; asiemiginowska@cfa.harvard.edu

<sup>2</sup> MIT Kavli Institute for Astrophysics & SpaceResearch 77 Massachusetts Ave.,Cambridge, MA 02139; ccheung@space.mit.edu

<sup>3</sup> Jansky Postdoctoral Fellow; National Radio Astronomy Observatory

<sup>4</sup> Steward Observatory, University of Arizona, Tucson, AZ

<sup>5</sup> Department of Physics, University of Bristol, Tyndall Ave., Bristol, UK

namic range, as evidenced, for example, by the discovery of many resolved quasar X-ray jets (e.g. Schwartz et al. 2000, Siemiginowska et al. 2002, Sambruna et al. 2004, Marshall et al. 2005).

The large-scale X-ray emission observed in radio sources can result from several processes, confusing detections of X-ray clusters at  $z > 1$  (e.g. Celotti & Fabian 2004). Radio synchrotron emission implies the presence of a population of relativistic particles that produce high-energy emission via inverse Compton scattering of the cosmic microwave background (CMB) photons. The energy density of the CMB increases with redshift as  $(1+z)^4$ , so the surface brightness of the inverse Compton emission is approximately constant with redshift. This is in contrast with thermal cluster emission where the surface brightness drops with redshift. X-ray spectral and spatial information are key to identifying different emission components and measuring diffuse thermal X-ray emission.

At the highest redshifts Carilli et al. (2002) describe extended emission possibly associated with thermal emission from shock-heated gas within  $\sim 150$  kpc of the  $z = 2.156$  radio galaxy PKS 1138-262. Fabian et al. (2003) report  $\sim 100$  kpc-scale emission around the nucleus of the redshift  $z = 1.786$  radio galaxy 3C 294 and give several possible explanations for the origin of this emission. In both cases the poor quality of the X-ray spectrum does not allow confirmation of the thermal nature of the diffuse X-ray emission. At redshifts  $0.5 < z < 1.0$  thermal confirmation has been possible in some sources, e.g. 3C 220.1 (Worrall et al. 2001)

Several deep images of nearby X-ray clusters (Fabian et al. 2003, Forman et al. 2003, Nulsen et al. 2004) obtained recently with *Chandra* provide evidence that intermittent AGN outbursts with an average power of  $\sim 10^{45}$  erg sec $^{-1}$  supply energy into the cluster preventing its cooling (McNamara et al. 2005). These deeply imaged clusters contain only relatively low power AGN ( $\sim 10^{40} - 10^{43}$  erg sec $^{-1}$ ) that are interpreted as having been active in the past in order to drive the observed cluster morphology. In contrast to these low redshift clusters, the 3C 186 cluster is observed during the quasar's active phase while heating the cluster medium.

3C 186 is a very luminous quasar ( $L_{bol} \sim 10^{47}$  erg sec $^{-1}$ ). It has a strong big blue bump in the optical-UV band and broad optical emission lines (Netzer et al. 1997, Simpson & Rawlings 2000, Kuraszkiewicz et al. 2002, Evans & Koratkar 2004). It is therefore a typical quasar except for its radio properties. The radio morphology shows two components separated by  $2''$  and a jet connecting the core and NW component (Cawthorne et al., 1986). Murgia et al. (1999) estimated the age of the CSS source to be of the order of  $\sim 10^5$  years based on the spectral age of the radio source. Our observation provides X-ray morphology and spectral information for the quasar and an associated X-ray cluster. The quasar core is so bright in X-rays that any X-ray emission associated with the radio components is not spatially resolved. The diffuse X-ray cluster emission is detected beyond the quasar core and

the CSS source.

We describe the *Chandra* observation, our analysis techniques and the results for the extended component in Sec.2. Section 3 and 4 present the archival radio and optical data. The quasar X-ray spectrum is presented in Sec.5. Section 6 contains the discussion.

Throughout this paper we use the cosmological parameters based on the WMAP measurements (Spergel et al. 2003):  $H_0 = 71$  km sec $^{-1}$  Mpc $^{-1}$ ,  $\Omega_M = 0.27$ , and  $\Omega_{vac} = 0.73$ . At  $z = 1.063$ ,  $1''$  corresponds to  $\sim 8.2$  kpc.

## 2. CHANDRA OBSERVATIONS

3C 186 was observed for  $\sim 38$  ksec with the *Chandra* Advanced CCD Imaging Spectrometer (ACIS-S, Weisskopf et al. 2002) on 2002 May 16 (ObsID 3098). The source was located  $\sim 35''$  from the default aim-point position (to avoid node boundaries) on the ACIS-S backside illuminated chip S3 (Proposer's Observatory Guide (POG)<sup>6</sup>). The 1/8 subarray CCD readout mode of one CCD only was used resulting in 0.441 sec frame readout time. The observation was made in VFAINT mode with the standard 5x5 pixel island used to assign the event grades by the pipeline. This mode allows for a more efficient way of determining the background events and cleaning the background, especially at the higher energies. After standard filtering the effective exposure time for this observation was 34,398 sec. Given the ACIS-S count rate of 0.025 counts s $^{-1}$  frame $^{-1}$  the pileup fraction was low  $< 2\%$  (see PIMMS<sup>7</sup>).

Figure 1 shows the *Chandra* ACIS-S image overlayed with the quasar core and background regions. Figure 2 shows the ACIS-S image of 3C 186 adaptively smoothed with the CIAO tool CSMOOTH. The X-ray emission is more extended than the X-ray emission of a typical radio-quiet quasar observed with *Chandra*. The diffuse emission extends up to  $\sim 120$  kpc in radius. Figure ?? show the smoothed images in soft (0.5-2 keV) and hard (2-7 keV) energy bands. Only the NE quadrant is visible in the hard band, while all of the extended emission is visible in the soft. Below we describe in detail the imaging and spectral analysis of this emission.

### 2.1. Imaging Analysis

The X-ray data analysis was performed in CIAO 3.2<sup>8</sup> with the calibration files from the CALDB 3.0 data base. Note that the ACIS-S contamination file `acisD1999-08-13contamN0003.fits` was included in our analysis; this accounts for the temporal, but not spatial, variation of the contamination layer on the optical-blocking filter of ACIS<sup>9</sup>. Since the quasar is observed close to the aim-point, which is where the spatially-invariant contamination model was calibrated, the results will not change if the data were re-analyzed using the spatially-dependent contamination model. We used *Sherpa* (Freeman et al. 2001) for all spectral and image modeling and fitting.

We ran `acis_process_events` to remove pixel randomization and to obtain the highest resolution image data. The X-ray position of the quasar (J2000: 07 44 17.47 +37

<sup>6</sup> <http://asc.harvard.edu/propser/POG/index.html>

<sup>7</sup> <http://asc.harvard.edu/toolkit/pimms.jsp>

<sup>8</sup> <http://cxc.harvard.edu/ciao/>

<sup>9</sup> <http://cxc.harvard.edu/ciao/why/acisqedeg.html>

53 17.11) agrees with the radio position (Li & Jin 1996) to better than  $0.1''$ , (which is smaller than *Chandra*'s 90% pointing accuracy of 0.6 arcsec, Weisskopf et al. 2003), so we have high confidence in the source identification.

To determine the size of the extended emission we ran a ray trace using CHaRT<sup>10</sup> and then MARX<sup>11</sup> to create a high S/N simulation of a point source. We modeled the quasar core as a point source with the energy spectrum given by the fitting described in Section 5. We then extracted a radial profile from both the *Chandra* data and the simulated point source image assuming annuli separated by 1 arcsec and centered on the quasar. For the simulation we added 7% errors to account for uncertainty in the raytrace model (Schwartz et al 2000a, Jerius et al 2004). The PSF was normalized to match the peak surface brightness of the core. The resultant profiles are shown in Fig 4 and clearly illustrate that the observed emission (empty squares) is highly inconsistent with a point source (solid line and empty triangles).

We apply a  $\beta$ -model to the one-dimensional surface brightness profile beyond  $\sim 3''$  radius to estimate a core radius and  $\beta$  parameter for the diffuse emission. The best fit model is represented in Figure 5 with  $\beta=0.64^{+0.11}_{-0.07}$  and a core radius  $r_c = 5.8''^{+2.1}_{-1.7}$  which corresponds to  $47^{+13}_{-14}$  kpc.

Since the core radius found in the one-dimensional analysis is small, a two-dimensional fit was made to see what influence the quasar emission and any non-sphericity of the cluster emission has on the  $\beta$ -model parameters. A model consisting of the CHaRT-generated PSF and a two-dimensional  $\beta$  model was fitted to the data, using the default pixel size of  $0.492''$ . The Cash statistic (Cash 1979) was used, since the number of counts per pixel was low outside the core, and the cluster center, ellipticity, and position angle were allowed to vary as well as the normalization, core radius, and  $\beta$  parameter. The best-fit cluster location differs from that of the quasar by  $0.2''$ , which is within the one-sigma error circle of the position ( $0.3''$ ). The best-fit model is elliptical, with an ellipticity of  $0.24^{+0.06}_{-0.07}$  and position angle of  $47 \pm 10$  degrees, but the core radius and  $\beta$  values are similar to the one-dimensional results, with  $r_c = 5.5^{+1.5''}_{-1.2}$  ( $45^{+12}_{-10}$  kpc) and  $\beta = 0.58^{+0.06}_{-0.05}$ .

## 2.2. Spectral Analysis of the Extended emission

We extracted the energy spectrum of the extended emission from an annulus of radii  $2.7''$  and  $15''$  centered on the quasar. There are  $1189 \pm 34$  total counts and  $741.4 \pm 40.4$  net source counts in this region in the full *Chandra* energy band. The background spectrum was taken from the annulus of radii  $20''$  and  $30''$ . Because the background increases at low and high energies we modeled only the spectrum within a 0.3-7 keV energy range. The total number of counts in this energy range was  $876 \pm 31$  with  $691.0 \pm 32.5$  net counts. In all spectral modeling we simultaneously fit background and source data applying  $\chi^2$  statistics with the weighting described by Primini et al. (1994) as implemented in *Sherpa*. All errors quoted below are 90% errors for a single parameter calculated with the *projection* routine in *Sherpa*. Table 1 lists the applied models and the best fit values.

<sup>10</sup> <http://cxc.harvard.edu/chart/>

<sup>11</sup> <http://space.mit.edu/CXC/MARX/>

<sup>12</sup> Stark et al 1992

We first fitted the spectrum of the diffuse emission with an absorbed power-law model assuming the equivalent column of hydrogen in the Galaxy of  $5.68 \times 10^{20}$  atoms  $\text{cm}^{-2}$  (COLDEN<sup>12</sup>). We then tested for excess absorption. The fitted absorbing column is in agreement with the Galactic value (see Table 1). Modeling the data with a power law indicated an excess at the Fe-line energy characteristic of thermal emission at the quasar redshift. We added a gaussian line to the model and obtained the line equivalent width of  $\text{EW}=412$  eV at the observed energy  $E_{\text{obs}}=3.18 \pm 0.07$  keV (90% errors) corresponding to the rest-frame energy of  $6.56 \pm 0.14$  keV. Note that this line energy indicated that the line is emitted by the hot ionized plasma.

We next applied the RAYMOND and MEKAL XSPEC plasma models in *Sherpa* and obtained gas temperatures  $4.4$ - $5.2$  keV for two choices of abundance, solar and 0.3 solar, using the abundances of Anders & Grevesse (1989). Figure 6 shows the best-fit thermal model together with the residuals. The observed unabsorbed flux assuming these models is of order  $6.2 \pm 0.3 \times 10^{-14}$  erg  $\text{sec}^{-1}$   $\text{cm}^{-2}$  for the 0.5-2 keV energy range and  $5 \pm 0.7 \times 10^{-14}$  erg  $\text{sec}^{-1}$   $\text{cm}^{-2}$  for the 2-10 keV energy range (the flux errors are based on 5% and 14% counts uncertainties in each band respectively).

The 0.5-2 keV rest frame X-ray luminosity of the cluster emission is equal to  $\sim 3 \times 10^{44}$  erg  $\text{sec}^{-1}$  (K-corrected). This is only the luminosity calculated based on the emission in the adopted annulus extending to about 122 kpc. This is about 52% of the total cluster luminosity as estimated from the radial profile fitting described in the previous section. Thus the total cluster luminosity is approximately  $\sim 6 \times 10^{44}$  erg  $\text{sec}^{-1}$ .

To investigate a possible non-thermal contribution to the spectrum due to inverse Compton scattering of CMB photons we fixed the MEKAL model at the best value and added a power law component with  $\Gamma = 1.7$  to the model. The  $3\sigma$  upper limit for the contribution of this component at 1 keV is then  $3.4 \times 10^{-6}$  photons  $\text{cm}^{-2}$   $\text{sec}^{-1}$ , i.e. less than 12% of the extended emission can be non-thermal.

To investigate possible temperature variations in the radial direction we extracted the spectra from two annuli: the inner one spans  $2.7''$ - $7.8''$  and the outer one spans  $7.8''$ - $15''$ . Table 2 summarizes the results. The hardness ratio indicates that there are more soft counts in the inner region than in the outer one. The RAYMOND model fit to these spectra indicate a slight temperature decrease, by  $\Delta kT \sim 0.3$  keV, towards the inner radii. However the errorbars are larger than any apparent deviations. The available data do not allow for fitting of cooling flow models (see Sec.6.1 for cooling-flow discussion).

To further investigate possible temperature variations of the extended emission in the azimuthal direction we divided the  $2.7''$  to  $15''$  annulus into four sectors and extracted counts and spectra from these sectors. The sectors, illustrated in Fig.7a, were chosen to follow the non-symmetrical shape of the extended emission as apparent in the smoothed image (Fig.2 and Fig.3). We calculated the surface brightness profile in each sector which confirmed

that the emission in the NE-SW direction (sectors 1 and 3) is stronger (by a factor of 1.25-1.5) than in NW-SE direction (sectors 4 and 2). The surface brightness values are indicated in Figure 7b.

The X-ray emission properties of the sectors are presented in Table 2. The hardness ratios indicate possible spectral differences between sectors. We fit the *Chandra* spectrum of each sector with a thermal emission model. There is a slight temperature variation (with a minimum of 3.7 keV and a maximum of 4.9 keV) between sectors in the best-fit values, however the error bars are approximately 1.5-2 keV, so that the fitted variations are all within 90% errors.

In summary, the diffuse emission is non-symmetric and elongated in the NE-SW direction with the harder emission towards NE (see Fig.3). Note that this structure is orthogonal to the radio emission described in the next section.

### 3. RADIO OBSERVATIONS

We searched for radio emission corresponding to the diffuse X-ray emission revealed in the *Chandra* image by re-analyzing VLA 1.5 GHz data published by van Breugel et al.. (1992). The multi-configuration (A and B) data were obtained in 1987 and amounted to a total integration time of about 80 minutes split almost equally between the two configurations. At the resolution of our image (Figure 8a), the radio source is dominated by a 1.8" double source aligned at a position angle of about -37 deg. Our self-calibrated dataset does not show extended radio emission on the scale of the X-ray emission detected above a  $3\sigma$  rms noise of 0.75 mJy/beam in the naturally weighted image; the off-source ( $>15''$ ) rms achieved in the image is about a factor of two smaller.

We also analyzed a 410 second VLA 15 GHz A configuration dataset of 3C 186 obtained on 13 Dec 1992 (program AL280) in order to examine the radio jet more clearly. The image shows similar features to previous high resolution maps (Cawthorne et al.. 1986; Spencer et al. 1991), i.e., a one-sided jet to the northwest connecting a flat-spectrum core to a diffuse radio lobe, and a bright radio lobe in the southeast direction (see Fig. 8b).

### 4. HUBBLE SPACE TELESCOPE DATA AND OPTICAL EMISSION

A cosmic-ray rejected WFPC2 Associations<sup>13</sup> image with a total integration time of 8,000 seconds was downloaded from the HST archive. The F675W image, obtained in Program 6491, was centered on one of the lower resolution wide field (WF) chips. We modeled the central source with elliptical isophotes utilizing the ELLIPSE task in the STSDAS<sup>14</sup> package and subtracted it from the image in order to show the nearest lying objects more clearly. The resultant image (Fig.9) shows several sources within the X-ray cluster emission indicated by a 15" circle. Unfortunately only a single band image of 3C 186 was taken with the WFPC2 camera and we cannot identify the colors of these sources.

### 5. QUASAR X-RAY EMISSION

<sup>13</sup> <http://archive.stsci.edu/hst/manual>

<sup>14</sup> [http://www.stsci.edu/resources/software\\_hardware/stsdas](http://www.stsci.edu/resources/software_hardware/stsdas)

The quasar core emission dominates the overall X-ray emission in the vicinity of 3C 186. We define the quasar emission region as a circle with 1.75" radius and assume background emission from an annulus with radii 20" and 30" (see Fig.1). Based on the PSF modeling we estimate that  $\sim 98\%$  of the point-source counts are included in this source region. The extracted quasar spectrum contains  $1968.7 \pm 44.3$  net counts (1905.4 net counts in energy range between 0.3-7 keV). We model the spectrum with an absorbed power law. The best-fit power-law model has a photon index  $\Gamma = 2.01 \pm 0.07$  and a 2-10 keV flux of  $1.7 \times 10^{-13}$  ergs cm $^{-2}$  sec $^{-1}$  which corresponds to a quasar X-ray luminosity  $L_X(2\text{-}10 \text{ keV}) = 1.2 \times 10^{45}$  erg sec $^{-1}$  and  $L_X(0.5\text{-}2 \text{ keV}) = 1.1 \times 10^{45}$  erg sec $^{-1}$  (unabsorbed and K-corrected luminosity). We do not detect any significant neutral absorbing column intrinsic to the quasar with the  $3\sigma$  upper limit to the equivalent column of Hydrogen of  $< 9.0 \times 10^{20}$  atoms cm $^{-2}$ .

The power-law fit to the data leaves some residuals at  $\sim 3$  keV indicating a possible emission line at this energy. We added the Gaussian line component to the model and obtained the best fit location for the narrow emission line (FWHM  $< 0.23$  keV) at  $E_{obs} = 3.07^{+0.06}_{-0.11}$  keV corresponding to  $E_{rest} = 6.33 \pm 0.06$  keV. The line equivalent width is equal to  $EW = 162$  eV and it can be identified with Fe-K $\alpha$  emission. The best-fit model and residuals are shown in Fig.10. (Note that the residuals between 1 and 2 keV are due to calibration uncertainties.) We can estimate the flux contribution to this line from the extended thermal emission by extrapolating the radial profile of the extended emission into the central circular region assumed for the quasar emission. The contribution from the thermal cluster emission to the quasar spectrum is of order 10%. Given the line flux in both components we estimate that only about  $\sim 5\%$  of the line emission can come from the thermal cluster emission, thus the line is dominated by the nuclear emission. Note that the energy,  $E_{rest} = 6.33 \pm 0.06$  keV, of the detected Fe-line in the quasar spectrum is in agreement with being emitted by the neutral medium, while the energy of the Fe-line emitted by the cluster gas,  $E_{rest} = 6.56 \pm 0.14$  keV, indicates an emission from ionized gas.

## 6. DISCUSSION

### 6.1. X-ray Cluster

Our *Chandra* observation reveals X-ray cluster emission at the redshift of the quasar 3C 186. The X-ray properties of the cluster are summarized in Table 3. We compare the cluster temperature and its luminosity with results for the other clusters at high redshift using the MEKAL model with the abundance set to 0.3 as in Vikhlinin et al.(2002). The cluster temperature of  $\sim 5.2^{+1.2}_{-0.9}$  keV and the total X-ray luminosity of  $L_X(0.5 - 2 \text{ keV}) \sim 6 \times 10^{44}$  erg sec $^{-1}$  agree with the temperature-luminosity relation typically observed in high redshift ( $z > 0.7$ ) clusters (e.g. Vikhlinin et al. 2002, Lumb et al. 2004).

We can estimate physical properties of the cluster using standard formulae (Donahue et al. 2003; Worrall &

Birkinshaw, 2004). Approximating the X-ray diffuse emission as spherical, we calculate the cluster central electron density ( $n_0$ ) to be approximately  $0.044 \pm 0.006 \text{ cm}^{-3}$  (errors are only due to the uncertainty in normalization) for the best-fit 1D beta model parameters:  $\beta=0.64$ , a core radius of  $\theta_c = 5.8''$  (Sec.2.1), a gas temperature of 5 keV and the spectral normalization of  $3.5(\pm 0.4) \times 10^{-4}$  based on the MEKAL model fit to the spectrum of the diffuse emission (assuming the annulus between  $2.7''$  and  $15''$  radii). These parameters imply that the mass of the gas enclosed within 1 Mpc radius of the isothermal sphere is  $\sim 2.2 \times 10^{13} M_\odot$ . The total gravitational mass enclosed within 1 Mpc is  $\sim 2.6 \times 10^{14} M_\odot$  assuming an isothermal-sphere model. The cluster gravitational mass is comparable to the mass of the other high redshift clusters recently measured with *Chandra* and *XMM-Newton* (Donahue et al. 2003, Worrall & Birkinshaw 2003, Vikhlinin et al 2002). The gas fraction, i.e.  $\sim 10\%$ , broadly agrees with the gas fraction usually found in high redshift ( $z > 0.7$ ) clusters.

We found a relatively small core radius,  $\sim 50$  kpc, for the 3C 186 cluster while most redshift  $z > 0.7$  clusters have typical core radii larger than 100 kpc. If gas of the same X-ray luminosity as found within a radius of 123 kpc of 3C 186 were distributed with a beta model of more typical core radius (150 kpc), the gas mass contained within a radius of 1 Mpc would increase by a factor of about 2.

Is there a cooling flow in this cluster? We estimate the gas mass enclosed within the core radius of  $\sim 50$  kpc to be of the order of  $2.2 \times 10^{11} M_\odot$ . Given the gas central density and the temperature of 5 keV the cooling time for this core is  $\sim 1.6 \times 10^9$  years and without a heat source there would be a cooling flow with the cooling-flow rate  $\sim 50 M_\odot \text{ yr}^{-1}$  (Fabian & Nulsen 1977, Fabian 1994).

Our image analysis indicates that the cluster X-ray emission follows an elliptical distribution (see Section 2.1). The angle between the major axes of the two-dimensional ellipse and the radio jet axes is  $\sim 84^{+7}_{-6}$  degrees. This type of X-ray vs. radio morphology is often seen in lower redshift clusters and it is interpreted as due to interactions between the radio plasma and the cluster medium (as for example in Hydra cluster in Nulsen et al 2002). The current radio data do not show any radio emission on scales similar to the observed X-ray cluster emission. However, the X-ray morphology suggests that there could be old plasma there possibly associated with previous activity of the quasar. The detection of a relic at low radio frequency observation would allow studies of the evolution timescales and the feedback between the quasar activity and the cluster medium.

## 6.2. Optical Environment of 3C 186

Optical observations of the quasar 3C 186 indicated that the source is located in a rich galaxy environment. Sánchez and González-Serrano (2002) studied an over-density and clustering of galaxies in the optical field of several high redshift radio sources. They include a K-band image of the 3C 186 field and indicate that the surface density of the galaxies in a possible cluster peaks to the NE about  $50''$  from the quasar. While the reported location of the peak density is located just outside the *Chandra* FOV we do not detect any significant X-ray emission towards the optical peak away from the quasar. In fact the quasar

seems to be centrally located with respect to the X-ray diffuse emission.

Recent optical study of the cluster environments of radio-loud quasars at  $0.6 < z < 1.1$  by Barr et al (2003) shows that these quasars do not reside in the center of the galaxy distributions. Because the X-ray emitting gas traces the cluster's gravitational potential, the X-ray observations can confirm whether the quasar is located in the center of the potential well of the cluster. The *Chandra* observations 3C 186 indicate that the quasar is located at the center of the X-ray emission and offset from the center of the galaxy distribution.

## 6.3. Lack of Confinement of the CSS source

The diffuse emission on a  $\sim 120$  kpc scale discovered in this *Chandra* observation indicates the presence of a hot Intercluster medium (ICM) surrounding this powerful CSS quasar. The X-ray spectrum of the cluster is dominated by a thermal component with a strong Fe-line at the quasar redshift. In one scenario the small size of CSS radio sources is associated with a dense environment that prevents the expansion of the source and confines the radio lobes to the size of a host galaxy (Wilkinson et al. 1981, van Breugel et al. 1984, O'Dea et al. 1991). Is this cluster then responsible for confining the CSS source?

Based on the cluster central density and temperature, we estimate a central thermal pressure of  $\sim 5 \times 10^{-11} \text{ dyn cm}^{-2}$ . If this pressure is higher than the pressure within the expanding radio components of the CSS source then the cluster gas may be responsible for confining the radio source and its small size.

The radio source is dominated by a double at 1.5 GHz, which straddles a central flat-spectrum radio core as seen in the higher resolution 15 GHz map (Figure 8). Using DIFMAP's MODELFIT (Shephard, Pearson & Taylor 1994) routine, the 1.5 GHz data are best-fit with two 0.59 Jy elliptical Gaussians with dimensions of  $0.7'' \times 0.3''$ , and a separation of  $1.8''$ . Taking the spectral index to be 1, and approximating each component as a homogeneous spheroid, we estimate the minimum pressure in each radio component to be  $\sim 10^{-8} \text{ dyn cm}^{-2}$  (see also Murgia et al 1999). Thus the radio source is highly overpressured by about 2-3 orders of magnitude with respect to the thermal cluster medium.

The new X-ray detection gives direct observational evidence that the radio source is not thermally confined as posited in the "frustrated" scenario for CSS sources. Instead, at least in this CSS quasar, it appears that the radio source may indeed be young (Readhead & Hewish 1976; Phillips & Mutel 1982, Carvalho 1985) and that we are observing an early stage of radio source evolution.

The jet can also interact and be stopped by a clumpy cold medium of the host galaxy, as described by Carvalho et al 1998, De Young 1991 or Jeyakumar et al 2005. The absorption due to this cold medium should be detectable in the quasar X-ray spectrum. We can use the  $3\sigma$  upper limit of  $9 \times 10^{20} \text{ cm}^{-2}$  on the total absorbing column density intrinsic to the quasar (see Sec.5 and Table 4) to estimate the total size of the clumpy medium. The *frustrated* jet models require clouds with densities of  $1-30 \text{ cm}^{-3}$ . The absorption limit gives the size of the clumpy medium of order 10-100 pc compared with the 16 kpc diameter of the

radio source. Any such region cannot significantly limit the expansion of the radio source and frustrate the jet (see also discussion in Guainazzi et al 2004).

Our X-ray observation of 3C 186 indicates that the CSS radio source is not confined, but it is at its early stage of the evolution into a large scale radio source.

#### 6.4. The CSS and the Cluster Heating

The CSS radio components are overpressured with respect to the thermal cluster gas. Thus the expansion of these components into the cluster medium could potentially heat the center of this cluster. The energy dissipated into the cluster by the expanding radio components has been widely discussed in the context of the low redshift clusters, where there is evidence for the repetitive outbursts of an AGN. However, the details of the dissipation process are undecided with ion viscosity and “sound” waves being possible candidates (Fabian et al. 2005). On the other hand the mechanical energy released during the shock wave propagation throughout the cluster could be transferred into the cluster thermal energy at the location of the shock (P.Nulsen private communication).

We can estimate the energy content of the hot cluster gas assuming a total emitting volume of  $2.3 \times 10^{71} \text{ cm}^3$  (contained by an annulus with 3 and 15" radii, assuming spherical geometry) and  $kT \sim 5 \text{ keV}$ , to be of the order of  $\frac{3}{2}kTnV \sim 2 \times 10^{61} \text{ ergs}$  (where  $n$  is the average gas particle density in the cluster). We can estimate the jet power from the relation between the radio luminosity and the jet power given by Willott et al (1999, Eq.(12)). Using the 151 MHz flux density of  $5.9 \times 10^{-24} \text{ erg sec}^{-1} \text{ cm}^{-2} \text{ Hz}^{-1}$  (Hales et al. 1993) which accounts for the total radio emission from the jet and hot spots (the core is already almost completely self-absorbed at 1.7 GHz, Spencer et al. 1991) the jet kinetic power is of order  $L_{jet} \sim 10^{46} \text{ erg sec}^{-1}$ . If the expanding radio source dissipated the jet’s energy,  $L_{jet} \sim 10^{46} \text{ erg sec}^{-1}$ , into the cluster’s central 120 kpc region then the heating time would be  $\sim 10^8$  years. We can also estimate the amount of mechanical work done by the jet and radio components during the expansion to the current radio size ( $2'' \times 0.3'' \sim 2.3 \times 10^{66} \text{ cm}^3$ ) as  $pdV \sim 10^{56} \text{ ergs}$ . If the expansion velocity is of the order of 0.1c then the radio source has been expanding for about  $5 \times 10^5$  years with an average power of  $6 \times 10^{42} \text{ erg sec}^{-1}$ . The estimated jet power is  $\sim 3$  orders of magnitude higher.

#### 6.5. X-ray emission of the core

The evolution of radio-source expansion within host galaxies and clusters has been considered by Heinz, Reynolds and Begelman (1998). They simulated interactions between a growing radio source and the interstellar and intergalactic medium. For the highly supersonic expansion of the young source a shock forms around the expanding source and it heats up the medium to X-ray temperatures. As a result a “cocoon” of hot medium surrounds the radio source. Depending on the density of the medium and the strength of the shock a source of the size of 16 kpc can emit  $\sim 10^{45} \text{ erg sec}^{-1}$  in the *Chandra* band.

The double CSS radio source and the radio jet remain unresolved in the *Chandra* observation of 3C 186. Thus the “cocoon” region is located within the unresolved X-ray core and thus could be giving a significant contribu-

tion to the total observed X-ray luminosity of  $10^{45} \text{ erg s}^{-1}$ . The amount of this contribution depends on the physical parameters of the expanding radio source and the ISM. A weak Fe-line is the only emission feature present in the otherwise featureless X-ray spectrum, however the observed spectral photon index is quite steep for a typical radio loud quasar (Elvis et al 1985, Bechtold et al 1994). We therefore estimated a possible thermal contribution to the quasar luminosity using the RAYMOND plasma model fits to the quasar spectrum. We concluded that about  $\sim 15\%$  of the 0.5-2 keV luminosity, e.g.  $1.5 \times 10^{44} \text{ erg sec}^{-1}$  could be due to the thermal emission. Of course there are other possible contribution to the observed X-ray spectrum from the radio jets knots and hot spots. Consistent theoretical modeling of the expansion and the emission of the jet components in the future may help in understanding their relative contributions to the X-ray spectrum. This is necessary in order to disentangle “true” quasar emission related directly to the accretion flow.

The quasar optical-UV (big blue bump) luminosity of  $5.7 \times 10^{46} \text{ erg sec}^{-1}$  (based on measurements in Simpson & Rawlings, 2000) is dominated by the typical quasar emission related to the accretion onto a supermassive black hole. We can therefore estimate the central black hole mass and required accretion rate based on that luminosity. Assuming that the quasar is emitting at the Eddington luminosity the black hole mass should be of the order  $\sim 4.5 \times 10^8 M_\odot$ . Based on CIV FWHM measurements of Kuraszkiewicz et al (2002) and the Vestergaard (2002) scaling relationship for the black hole mass, the estimated mass of the black hole is approximately a factor of 10 higher,  $\sim 3.2 \times 10^9 M_\odot$ . In any case the accretion rate required by the observed UV luminosity, and assuming 10% efficiency of converting the gravitational energy into radiation, is equal to  $\sim 10 M_\odot \text{ year}^{-1}$ . Given the age of the radio source of  $5 \times 10^5$  years, a total of  $\sim 5 \times 10^6 M_\odot$  should have been accreted onto the black hole to support the current “outburst”.

Recent studies of formation of galaxies and growth of a supermassive black hole suggest that the quasar activity is a result of a merger event (e.g. DiMatteo, Springel & Hernquist 2005). In this model a short phase of quasar activity is a direct consequence of the increased fuel supply onto a central black hole. Based on the radio aging and the current size of 3C 186 its activity started  $\sim 10^6$  years ago. The X-ray cluster emission of 3C 186, although elliptical in shape does not show any signatures of a merger event responsible for that activity. The cooling time for this cluster is  $\sim 10^9$  years, so if this cluster is forming then the gas flowing into the center could onset the radio activity (Bremer et al. 1997). Such a powerful outburst can easily prevent the cooling of the cluster core. Although, the exact process of transferring the outburst energy into the cluster gas is unknown, the available outburst energy exceeds by  $> 2$  orders of magnitude the luminosity of the cluster core. The feedback between the jet heating and the cooling of the cluster can regulate the growth of the central black hole. On the other hand the short timescale of the current outburst may also suggest that the intermittent AGN behaviour could be related to the physics of the accretion flow (Siemiginowska, Czerny & Kostyunin 1996, Janiuk et al 2004) instead of the properties of a large scale

environment triggering the quasar outburst. This is the first cluster observed at the early phase of the quasar radio activity giving us a potential to study the early stages of interactions between the cluster and AGN.

### 6.6. Old halo: relic

Is the current 3C 186 outburst the first phase of the quasar activity in this cluster? The large mass of the central black hole suggests that the supermassive black hole must have been formed much earlier than  $10^5$  years ago. As we show in the previous section only a small fraction of the mass has been accreted during the current active phase.

One way to accommodate the observed statistics of source sizes in the radio source evolution is to invoke intermittent activity (Reynolds & Begelman 1997) with average timescales of  $\sim 10^4 - 10^5$  yrs. In this scenario, a diffuse radio halo filled with old electrons from previous periods of activity should be apparent around CSS sources like 3C 186 in deep, low-frequency radio maps. Most CSS and GPS sources do not show very large-scale (100's kpc) extended radio emission in present data (O'Dea 1998 and references therein). X-ray observations of nearby clusters suggest a longer period of the intermittency, e.g.  $10^6 - 10^7$  years (e.g. Fabian et al 2003, Forman et al 2004). For these longer timescales 3C 186 would still be at an early phase of the cycle.

If there was a previous outburst we might be able to detect “bubbles” filled with the old radio plasma (seen as depressions in the X-ray surface brightness) in deeper X-ray observations in the future. The “bubbles” observed in nearby clusters indicate locations of radio plasma injected into the cluster in the past (Churazov et al 2001). They are buoyant, moving within the cluster gas and last for at least one cycle, as indicated by more than one pair of “bubbles” observed in some X-ray clusters (Fabian et al. 2002, Belsole et al 2001, Owen et al. 2000). Even if the radio source outburst lasted only  $\sim 10^5$  years the radio plasma would still be present within buoyant “bubbles” loosing its energy via synchrotron radiation. Thus if there was a previous outburst we might be able to detect the radio relic in low-frequency observations.

At large redshifts, large-scale radio halos may produce a non-thermal X-ray component via inverse Compton scattering off the CMB. In the case of 3C 186, at  $z=1.063$ , the X-ray spectral fits do not require such a power-law component in addition to the thermal emission. From our data (Sec.2.2), we estimate that a non-thermal component contributes less than 12% of the total emission,  $F(1 \text{ keV}) \sim \text{few nJy}$ .

No large-scale extended radio emission is visible in our 1.5 GHz VLA image – we estimate that there is less than 0.3 Jy coming from a possible halo by integrating the  $3\sigma$  rms limit over the extent of the detected X-ray emission ( $\sim 15''$ ). The electrons scattering CMB photons to 1 keV ( $\gamma \sim 10^3$ ) radiate synchrotron radio emission at much lower

frequencies ( $\nu \sim (B / 1 \mu\text{G}) \text{ MHz}$ ). A deep low-frequency radio observation aimed at detecting extended radio emission on the scale of the X-ray cluster would put a useful lower limit on the cluster magnetic field assuming equipartition (see Carilli & Taylor 2002).

## 7. SUMMARY

Our main results can be summarize as follows:

- 1 We have observed the CSS quasar 3C 186 for 38 ksec and detected X-ray cluster emission extending out to  $\sim 120$  kpc from the quasar.
- 2 The cluster temperature and luminosity follows the relationship observed in the other high redshift clusters, its gas mass is relatively small. The low mass could be the result of a small core radius measured in this cluster in comparison to the other clusters at  $z > 0.7$ .
- 3 The estimated pressure of the cluster gas is 2-3 order of magnitude lower than the pressure of the radio components, thus the cluster gas cannot confine the expanding radio source.
- 4 Non-thermal and thermal emission associated with the radio components cannot be separated spatially from the unresolved X-ray emission that is measured. We have placed an upper limit of  $1.5 \times 10^{44} \text{ erg sec}^{-1}$  on the contribution from the gas that is shock heated as a result of the radio-source expansion. Detailed modeling is required to estimate the relative contribution of several possible components identified in radio observations.
- 5 Future low frequency radio observation may provide information about the large scale distribution of an old electron population from a previous outburst of the quasar activity in this source.

We thank Paul Nulsen and Brian McNamara for useful discussions. We thank the anonymous referee for a careful reading of the manuscript and comments. This research is funded in part by NASA contract NAS8-39073. Partial support for this work was provided by the National Aeronautics and Space Administration through Chandra Award Number GO-01164X and GO2-3148A issued by the Chandra X-Ray Observatory Center, which is operated by the Smithsonian Astrophysical Observatory for and on behalf of NASA under contract NAS8-39073. The VLA is a facility of the National Radio Astronomy Observatory is operated by Associated Universities, Inc. under a cooperative agreement with the National Science Foundation.

This work was supported in part by NASA grants GO2-3148A, GO-09820.01-A and NAS8-39073.

## REFERENCES

Alexander, P. 2000, MNRAS, 319, 8  
 Anders E. & Grevesse N. 1989, Geochimica et Cosmochimica Acta 53, 197  
 Barr, J. M., Bremer, M. N., Baker, J. C., & Lehnert, M. D. 2003, MNRAS, 346, 229  
 Baum, S. A., O'Dea, C. P., de Bruyn, A. G., & Murphy, D. W. 1990, A&A, 232, 19

Bechtold, J., et al. 1994, AJ, 108, 759

Belsole, E., et al. 2001, A&A, 365, L188

Bicknell, G. V., Dopita, M. A., & O'Dea, C. P. 1997, ApJ, 485, 112

Bremer, M. N., Fabian, A. C., & Crawford, C. S. 1997, MNRAS, 284, 213

Cash, W. 1979, ApJ, 228, 939

Carilli, C. L., Harris, D. E., Pentericci, L., Röttgering, H. J. A., Miley, G. K., Kurk, J. D., & van Breugel, W. 2002, ApJ, 567, 781

Carilli, C. L., & Taylor, G. B. 2002, ARA&A, 40, 319

Carvalho, J. C. 1985, MNRAS, 215, 463

Carvalho, J. C. 1998, A&A, 329, 845

Cawthorne, T. V., Scheuer, P. A. G., Morison, I., & Muxlow, T. W. B. 1986, MNRAS, 219, 883

Celotti, A. & Fabian, A. C. 2004, MNRAS, 261

Crawford, C. S. & Fabian, A. C. 2003, MNRAS, 339, 1163

Churazov, E., Brüggen, M., Kaiser, C. R., Böhringer, H., & Forman, W. 2001, ApJ, 554, 261

De Young, D. S. 1991, ApJ, 371, 69

Di Matteo, T., Springel, V., & Hernquist, L. 2005, Nature, 433, 604

Donahue, M., Gaskin, J. A., Patel, S. K., Joy, M., Clowe, D., & Hughes, J. P. 2003, ApJ, 598, 190

Elvis, M., Fiore, F., Wilkes, B., McDowell, J., & Bechtold, J. 1994, ApJ, 422, 60

Elvis, M., Wilkes, B. J., & Tananbaum, H. 1985, ApJ, 292, 357

Ellingson, E., Yee, H. K. C., & Green, R. F. 1991, ApJ, 371, 49

Evans, I. N., & Koratkar, A. P. 2004, ApJS, 150, 73

Yee, H. K. C. & Ellingson, E. 1993, ApJ, 411, 43

Fabian, A. C., Reynolds, C. S., Taylor, G. B., & Dunn, R. J. H. 2005, MNRAS, submitted (astro-ph/0501222)

Fabian, A. C. 1994, ARA&A, 32, 277

Fabian, A. C., Sanders, J. S., Crawford, C. S., & Ettori, S. 2003, MNRAS, 341, 729

Fabian, A. C., Sanders, J. S., Allen, S. W., Crawford, C. S., Iwasawa, K., Johnstone, R. M., Schmidt, R. W., & Taylor, G. B. 2003, MNRAS, 344, L43

Fabian, A. C., Celotti, A., Blundell, K. M., Kassim, N. E., & Perley, R. A. 2002, MNRAS, 331, 369

Fabian, A. C., & Nulsen, P. E. J. 1977, MNRAS, 180, 479

Fanti, C., Fanti, R., Dallacasa, D., Schilizzi, R. T., Spencer, R. E., & Stanghellini, C. 1995, A&A, 302, 317

Forman, W. et al astro-ph/0312576

Freeman, P., Doe, S., & Siemiginowska, A. 2001, Proc. SPIE, 4477, 76

Guainazzi, M., Siemiginowska, A., Rodriguez-Pascual, P., & Stanghellini, C. 2004, A&A, 421, 461

Gugliucci, N. E., Taylor, G. B., Peck, A. B., & Giroletti, M. 2005, ApJ, 622, 136

Hales, S. E. G., Baldwin, J. E., & Warner, P. J. 1993, MNRAS, 263, 25

Hardcastle, M. J., & Worrall, D. M. 1999, MNRAS, 309, 969

Heinz, S., Reynolds, C. S., & Begelman, M. C. 1998, ApJ, 501, 126

Janiuk, A., Czerny, B., Siemiginowska, A., & Szczerba, R. 2004, ApJ, 602, 595

Jerius, D. H., Gaetz, T. J., & Karovska, M. 2004, Proc. SPIE, 5165, 433

Jeyakumar, S., Wiita, P. J., Saikia, D. J., & Hooda, J. S. 2005, A&A, 432, 823

Kuraszkiewicz, J. K., Green, P. J., Forster, K., Aldcroft, T. L., Evans, I. N., & Koratkar, A. 2002, ApJS, 143, 257

Li, J. & Jin, W. 1996, A&AS, 120, 201

Lister, M. L. 2003, ASP Conf. Ser. 300: Radio Astronomy at the Fringe, 71

Lumb, D. H., et al. 2004, A&A, 420, 853

Marshall, H. L., et al. 2005, ApJS, 156, 13

Murgia, M., Fanti, C., Fanti, R., Gregorini, L., Klein, U., Mack, K.-H., & Vigotti, M. 1999, A&A, 345, 769

McNamara B. R.; Nulsen, P. E. J.; Wise, M. W.; Rafferty, D. A.; Carilli, C.; Sarazin, C. L.; Blanton, E. L. 2005, Nature, astro-ph/0411553

Netzer, H., et al. 1996, MNRAS, 279, 429

Nulsen, P. E. J.; McNamara, B. R.; Wise, M. W.; David, L. P., 2004, astro-ph/0408315

Nulsen, P. E. J., David, L. P., McNamara, B. R., Jones, C., Forman, W. R., & Wise, M. 2002, ApJ, 568, 163

O'Dea, C. P., De Vries, W. H., Worrall, D. M., Baum, S. A., & Koekemoer, A. 2000, AJ, 119, 478

O'Dea, C. P. 1998, PASP, 110, 493

O'Dea, C. P., & Baum, S. A. 1997, AJ, 113, 148

O'Dea, C. P., Baum, S. A., & Stanghellini, C. 1991, ApJ, 380, 66

Owen, F. N., Eilek, J. A., & Kassim, N. E. 2000, ApJ, 543, 611

Owsianik, I., Conway, J. E., & Polatidis, A. G. 1998, A&A, 336, L37

Phillips, R. B., & Mutel, R. L. 1982, A&A, 106, 21

Polatidis, A. G., & Conway, J. E. 2003, Publications of the Astronomical Society of Australia, 20, 69

Readhead, A. C. S., & Hewish, A. 1976, MNRAS, 176, 571

Readhead, A. C. S., Taylor, G. B., Xu, W., Pearson, T. J., Wilkinson, P. N., & Polatidis, A. G. 1996, ApJ, 460, 612

Readhead, A. C. S., Taylor, G. B., Pearson, T. J., & Wilkinson, P. N. 1996, ApJ, 460, 634

Reynolds, C. S., & Begelman, M. C. 1997, ApJ, 487, L135

Reynolds, C. S., McKernan, B., Fabian, A. C., Stone, J. M., & Vernaleo, J. C. 2005, MNRAS, 357, 242

Roychowdhury, S., Ruszkowski, M., Nath, B. B., & Begelman, M. C. 2004, ApJ, 615, 681

Ruszkowski, M., Brüggen, M., & Begelman, M. C. 2004, ApJ, 611, 158

Sambrook, R. M., Gambill, J. K., Maraschi, L., Tavecchio, F., Cerutti, R., Cheung, C. C., Urry, C. M., & Chartas, G. 2004, ApJ, 608, 698

Sánchez, S. F., & González-Serrano, J. I. 2002, A&A, 396, 773

Schoenmakers, A. P., de Bruyn, A. G., Röttgering, H. J. A., & van der Laan, H. 1999, A&A, 341, 44

Schwartz, D. A., et al. 2000, ApJ, 540, L69

Schwartz, D. A., et al. 2000a, Proc. SPIE, 4012, 28

Silk, J., & Rees, M. J. 1998, A&A, 331, L1;

Siemiginowska, A., Czerny, B., & Kostyunin, V. 1996, ApJ, 458, 491

Siemiginowska, A., et al. 2003, ApJ, 595, 643

Siemiginowska, A., Bechtold, J., Aldcroft, T. L., Elvis, M., Harris, D. E., & Dobrzański, A. 2002, ApJ, 570, 543

Simpson, C., & Rawlings, S. 2000, MNRAS, 317, 1023

Shepherd, M. C., Pearson, T. J., & Taylor, G. B. 1994, BAAS, 26, 987

Snellen, I. A. G., Schilizzi, R. T., Miley, G. K., de Bruyn, A. G., Bremer, M. N., & Röttgering, H. J. A. 2000, MNRAS, 319, 445

Spencer, R. E., et al. 1991, MNRAS, 250, 225

Spergel, D. N., et al. 2003, ApJS, 148, 175

Stanghellini, C., Dallacasa, D., O'Dea, C. P., Baum, S. A., Fanti, R., & Fanti, C. 2001, A&A, 377, 377

Stanghellini, C., O'Dea, C. P., Dallacasa, D., Baum, S. A., Fanti, R., & Fanti, C. 1998, A&AS, 131, 303

Stanghellini, C., Baum, S. A., O'Dea, C. P., & Morris, G. B. 1990, A&A, 233, 379

Stark, A. A., Gammie, C. F., Wilson, R. W., Bally, J., Linke, R. A., Heiles, C., & Hurwitz, M. 1992, ApJS, 79, 77

van Breugel, W. J. M., Fanti, C., Fanti, R., Stanghellini, C., Schilizzi, R. T., & Spencer, R. E. 1992, A&A, 256, 56

van Breugel, W., Miley, G., & Heckman, T. 1984, AJ, 89, 5

Vestergaard, M. 2002, ApJ, 571, 733

Vikhlinin, A., VanSpeybroeck, L., Markevitch, M., Forman, W. R., & Grego, L. 2002, ApJ, 578, L107

Voit, G. M., Balogh, M. L., Bower, R. G., Lacey, C. G., & Bryan, G. L. 2003, ApJ, 593, 272

Weisskopf, M. C., et al. 2003, Experimental Astronomy, 16, 1

Weisskopf, M. C., Brinkman, B., Canizares, C., Garmire, G., Murray, S., & Van Speybroeck, L. P. 2002, PASP, 114, 1

Wilkinson, P. N., Booth, R. S., Cornwell, T. J., & Clark, R. R. 1984, Nature, 308, 619

Willott, C. J., Rawlings, S., Blundell, K. M., & Lacy, M. 1999, MNRAS, 309, 1017

Worrall, D. M., Birkinshaw, M., Hardcastle, M. J., & Lawrence, C. R. 2001, MNRAS, 326, 1127

Worrall, D. M., & Birkinshaw, M. 2003, MNRAS, 340, 1261

Worrall, D. M., & Birkinshaw, M., 2004, to appear as a book chapter in 'Physics of Active Galactic Nuclei at all Scales', eds. D. Alloin, R. Johnson, P. Lira, (Springer Verlag), Lecture Notes in Physics series. astro-ph/0410297

Worrall, D. M., Hardcastle, M. J., Pearson, T. J., & Readhead, A. C. S. 2004, MNRAS, 347, 632

TABLE 1  
SPECTRAL MODELS OF THE X-RAY DIFFUSE EMISSION

Model <sup>a</sup>	N <sub>H</sub> or z	Abund Solar	Γ	Temp keV	Norm <sup>b</sup> 10 <sup>-5</sup>	χ <sup>2</sup> <sup>c</sup> (DOF)
PL	9.15 <sup>+5.12</sup> <sub>-3.89</sub>	-	2.06 <sup>+0.27</sup> <sub>-0.22</sub>	-	3.08 <sup>+0.66</sup> <sub>-0.48</sub>	79.92 (73)
PL+Gaussian Line E <sub>l</sub> <sup>d</sup> = 3.18±0.07 EW=412.7eV		-	2.12 <sup>+0.12</sup>		3.06 <sup>+0.21</sup>	68.69 (71)
RAYMOND	-	1		4.6 <sup>+1.1</sup> <sub>-0.7</sub>	30.2 <sup>+2.3</sup> <sub>-2.3</sub>	73.7 (74)
RAYMOND	-	0.3	-	5.2 <sup>+1.3</sup> <sub>-0.9</sub>	34.8 <sup>+3.1</sup> <sub>-3.0</sub>	74.0 (74)
RAYMOND	1.11 <sup>+0.04</sup> <sub>-0.03</sub>	0.3		5.4 <sup>+1.4</sup> <sub>-1.0</sub>	36.3 <sup>+3.4</sup> <sub>-3.5</sub>	71.1(74)
MEKAL	-	1	-	4.6 <sup>+1.1</sup> <sub>-0.7</sub>	29.8 <sup>+2.2</sup> <sub>-2.2</sub>	71.9 (74)
MEKAL	-	0.3	-	5.2 <sup>+1.3</sup> <sub>-0.9</sub>	34.6 <sup>+3.0</sup> <sub>-3.0</sub>	73.7 (74)

<sup>a</sup> All models except the first PL model include equivalent Hydrogen column of  $5.68 \times 10^{20}$  cm<sup>-2</sup> in the Milky Way from COLDEN; <sup>b</sup> Normalization in 10<sup>-5</sup> photons cm<sup>2</sup> sec<sup>-1</sup> at 1 keV for a power law model; for thermal models the normalization is defined as  $Norm \times 10^{-14} / (4\pi(D(1+z))^2) \int n_e n_H dV$  following the definitions of RAYMOND and MEKAL models in XSPEC, abundance table set to Anders & Grevesse (1989); <sup>c</sup> χ<sup>2</sup> following Primini et al in *Sherpa*; <sup>d</sup> Energy of the emission line in keV.

TABLE 2  
SPATIAL MODELS OF THE X-RAY DIFFUSE EMISSION

Region	Counts Tot	Net Counts Tot	Net Counts 0.3-7keV	Soft 0.5-2keV	Hard 2-10keV	Soft/Hard
Entire Annulus 2.7''-15''	1189±35	741.1±40.5	691.0±32.5	562.1 <sup>+31.1</sup> <sub>-30.3</sub>	143.9 <sup>+20.9</sup> <sub>-20.0</sub>	3.9 <sup>+0.6</sup> <sub>-0.8</sub>
Inner Annulus 2.7''-7.8''	490±22	392.9±24.2	379.3±21.4	317.2 <sup>+20.9</sup> <sub>-21.4</sub>	63.2 <sup>+10.6</sup> <sub>-11.3</sub>	5.2 <sup>+0.9</sup> <sub>-1.2</sub>
Outer Annulus 7.8''-15''	699±26	348.2±32.4	311.6±24.5	247.1 <sup>+21.7</sup> <sub>-21.8</sub>	82.8 <sup>+16.9</sup> <sub>-16.3</sub>	3.1 <sup>+0.4</sup> <sub>-0.6</sub>
Sector 1	206±14	142.1±16.4	128.1±13.4	100.4 <sup>+15.5</sup> <sub>-16.0</sub>	37.6 <sup>+8.1</sup> <sub>-8.9</sub>	2.8 <sup>+0.7</sup> <sub>-0.9</sub>
Sector 2	430±21	272.2±24.2	246.1±19.3	200.9 <sup>+22.9</sup> <sub>-23.1</sub>	60.6 <sup>+11.7</sup> <sub>-12.2</sub>	3.4 <sup>+0.5</sup> <sub>-0.7</sub>
Sector 3	164±13	111.2±14.7	107.6±12.3	96.7 <sup>+15.2</sup> <sub>-15.6</sub>	11.9 <sup>+5.5</sup> <sub>-6.2</sub>	10.4 <sup>+1.1</sup> <sub>-6.1</sub>
Sector 4	395±20	230.8±23.6	219.6±18.8	181.4 <sup>+16.8</sup> <sub>-17.5</sub>	34.7 <sup>+10.5</sup> <sub>-10.6</sub>	5.7 <sup>+1.2</sup> <sub>-2.2</sub>

TABLE 3  
SUMMARY OF SPATIAL AND SPECTRAL FITS TO DIFFUSE X-RAY EMISSION

Parameter	Property
β-model (1D)	$\beta=0.64^{+0.11}_{-0.07}$ , $r_c=5.8^{+2.1''}_{-1.7''}$
β-model (2D)	$\beta=0.58^{+0.06}_{-0.05}$ , $r_c=5.5^{+1.5''}_{-1.2''}$ ellipticity = $0.24^{+0.06}_{-0.07}$ , PA=47±10 degrees
$E_{\text{obs}}$ (Fe-line)	3.18±0.07 keV
EW (Fe-line)	412 eV
$F_{\text{obs}}$ (0.5-2 keV)	$6.2 \pm 0.3 \times 10^{-14}$ erg sec <sup>-1</sup> cm <sup>-2</sup>
$F_{\text{obs}}$ (2-10 keV)	$5.0 \pm 0.7 \times 10^{-14}$ ergs sec <sup>-1</sup> cm <sup>-2</sup>
$F_{\text{nonthermal}}$ (1 keV)	$<5.4 \times 10^{-15}$ erg sec <sup>-1</sup> cm <sup>-2</sup>
$L_{\text{tot}}$ (0.5-2 keV)	$6 \times 10^{44}$ erg sec <sup>-1</sup>

Fluxes are unabsorbed. Luminosities are K-corrected and in the source frame. (see text).

TABLE 4  
QUASAR MODELS

Model <sup>a</sup>	$N(z_{qso})^b$	$\Gamma$	Flux <sup>c</sup> [1 keV]	$E_{line}$ [keV]	$EW_{line}$ [eV]	$\chi^2$ (DOF) <sup>d</sup>
Power Law	$< 9.0^e$	$2.01 \pm 0.07$	$7.52 \pm 0.32$			138.2 (137)
PL+Gaussian Line		$2.03 \pm 0.07$	$7.48 \pm 0.28$	$^{+0.07}_{-0.16}$	130	132.1 (135)

<sup>a</sup> model assumes  $5.68 \times 10^{20}$  atoms  $\text{cm}^{-2}$  equivalent Hydrogen column in the Milky Way from COLDEN;

<sup>b</sup> absorbing column intrinsic to the quasar at  $z=1.063$  in units of  $10^{20}$  atoms  $\text{cm}^{-2}$ ;

<sup>c</sup> flux in units of  $10^{-5}$  photons  $\text{cm}^{-2}$   $\text{sec}^{-1}$   $\text{keV}^{-1}$  <sup>d</sup>  $\chi^2$  following formulation of Primini et al. in *Sherpa*; <sup>e</sup>  $3\sigma$  upper limit.

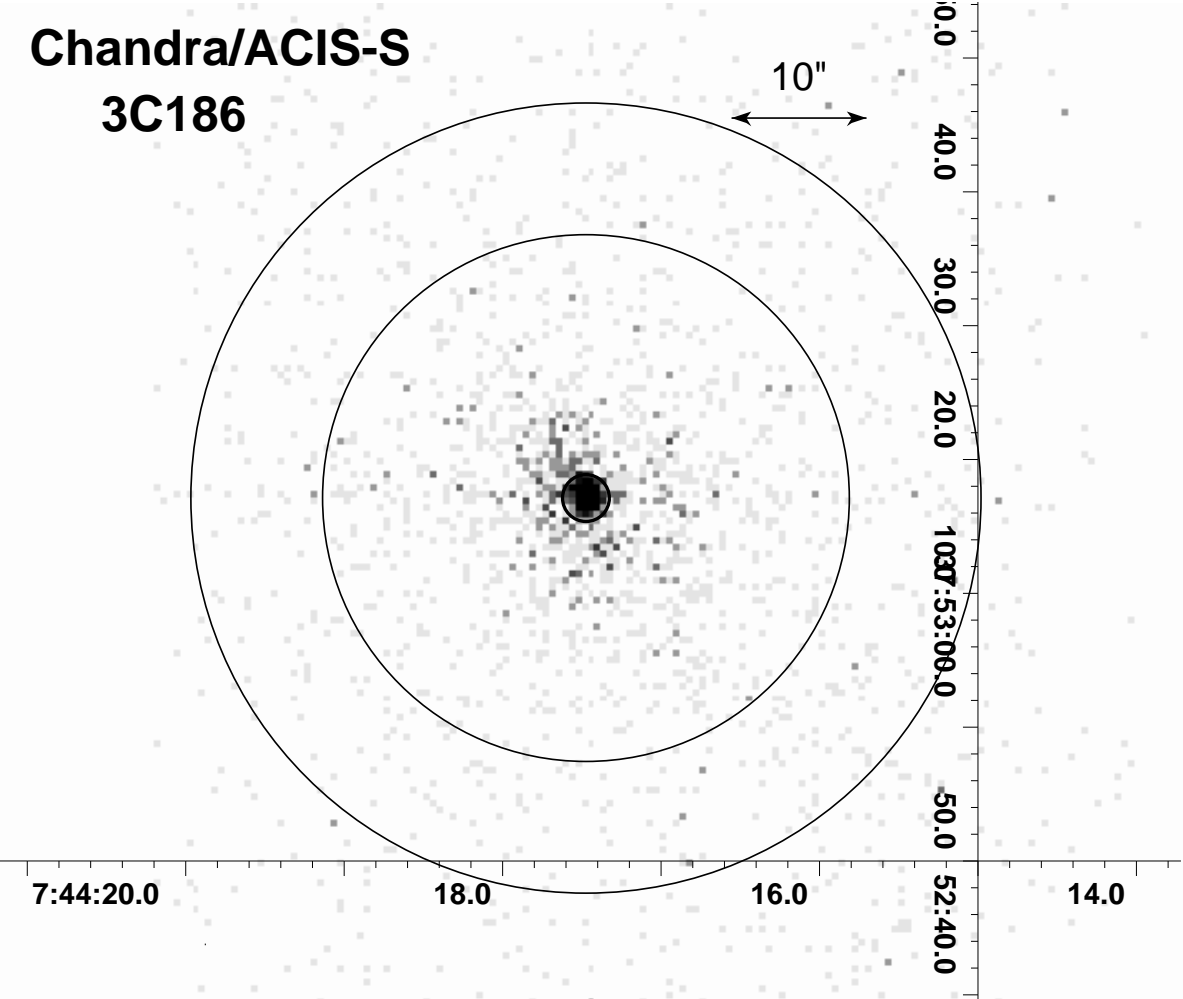


FIG. 1.— *Chandra* ACIS-S X-ray (0.3-7 keV) image of 3C 186. The pixel size is the standard ACIS-S pixel of  $0.492''$ . The quasar source region assumed for extracting the spectrum is a  $1.75''$  radius circle in the center of the field. The outer annulus with  $20''$  and  $30''$  radii illustrates the background region. The arrow in the upper right corner indicates the  $10''$  scale. North is up and East is left. Coordinates are J2000.

FIG. 2.— Adaptively smoothed exposure corrected image (photons energies within 0.3-7 keV range) of the *Chandra* ACIS-S observation of 3C 186 (Q0740+380). The diffuse emission is detected on  $> 100$  kpc scale,  $1''=8.2$  kpc. North is up and East is left. Contours represent a surface brightness of:  $(0.046, 0.066, 0.13, 0.2, 0.33, 0.46, 0.66, 6.635, 33.175) \times 10^{-6}$  photons  $\text{cm}^{-2}$   $\text{arcsec}^{-2}$ . The direction of the CCD readout is indicated by arrow on the right side. A blue arrow in the upper right corner shows the PA=-37 deg of the  $2''$  radio jet (see Fig 8).

FIG. 3.— Adaptively smoothed exposure corrected image of the *Chandra* ACIS-S observation 3C 186 (Q0740+380) in two X-ray bands: (1) soft 0.5-2 keV on the left and (2) hard 2-7 keV on the right. North is up and East is left. Contours represent a surface brightness of:  $(0.036, 0.066, 0.11, 0.3, 0.66, 6.635, 33.175) \times 10^{-6}$  photons  $\text{cm}^{-2}$   $\text{arcsec}^{-2}$ .  $1''=8.2$  kpc.

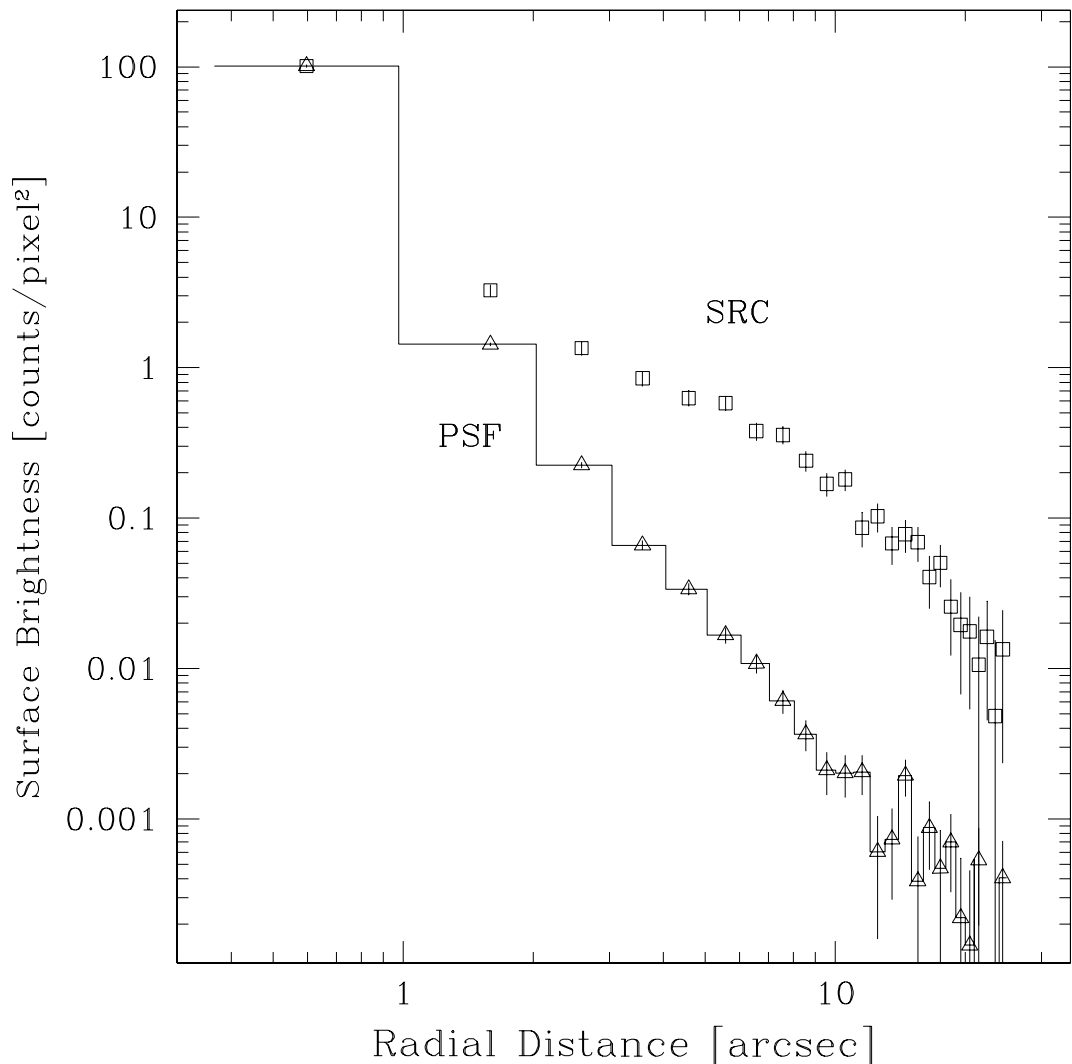


FIG. 4.— The background subtracted surface brightness profile up to  $25''$  distance from the quasar. The source data is indicated by the square points. The solid line with triangular points represents the simulated PSF profile.

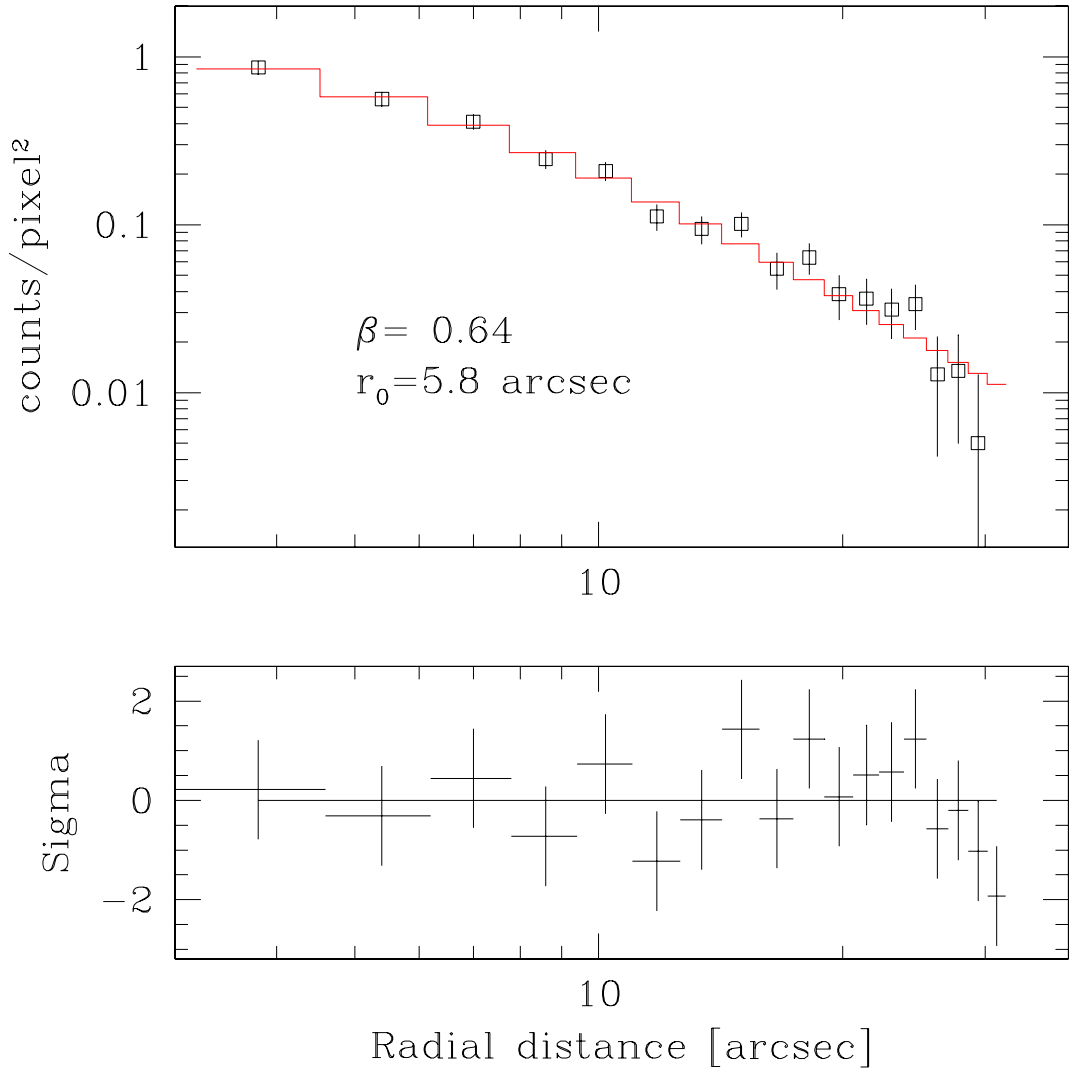


FIG. 5.— Background subtracted surface brightness profile for radii  $3''$  to  $30''$  fit with a beta model. The data are indicated by the square points. The solid line shows the best fit model with parameter  $\beta = 0.64^{+0.11}_{-0.07}$  and a core radius of  $r_{core} = 5.8''^{+2.1}_{-1.7}$ . The bottom panel illustrates the differences between the data and the model in units of  $\sigma$ .

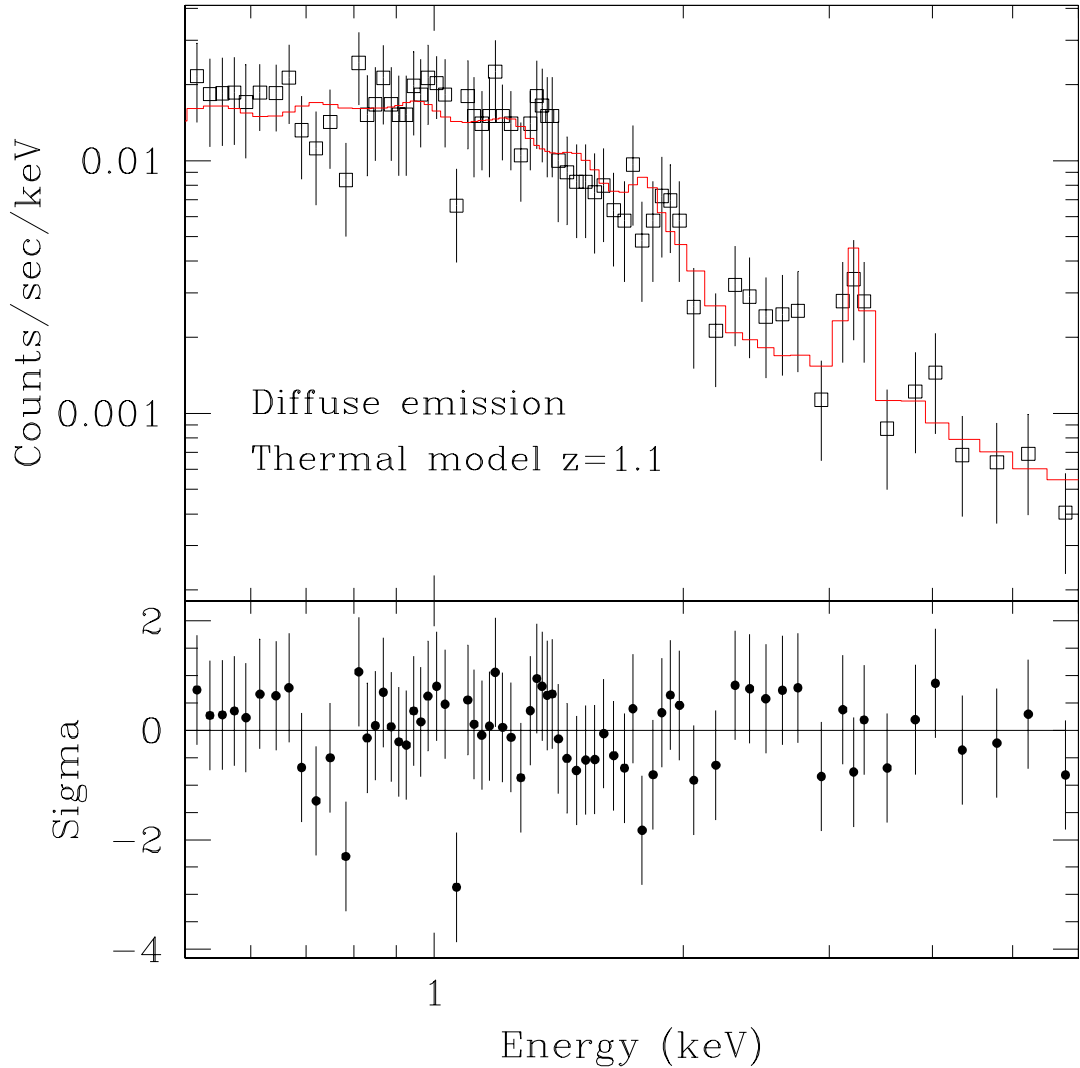


FIG. 6.— ACIS-S spectrum of the diffuse emission between 2.7 and 15 arcsec which we fit with the plasma model. Upper panel shows the data indicated by squares with  $1\sigma$  error-bars and the best-fit model drawn with a solid line. The bottom panel shows the residual difference between model and the data in units of sigma. The scatter is due to calibration uncertainties.

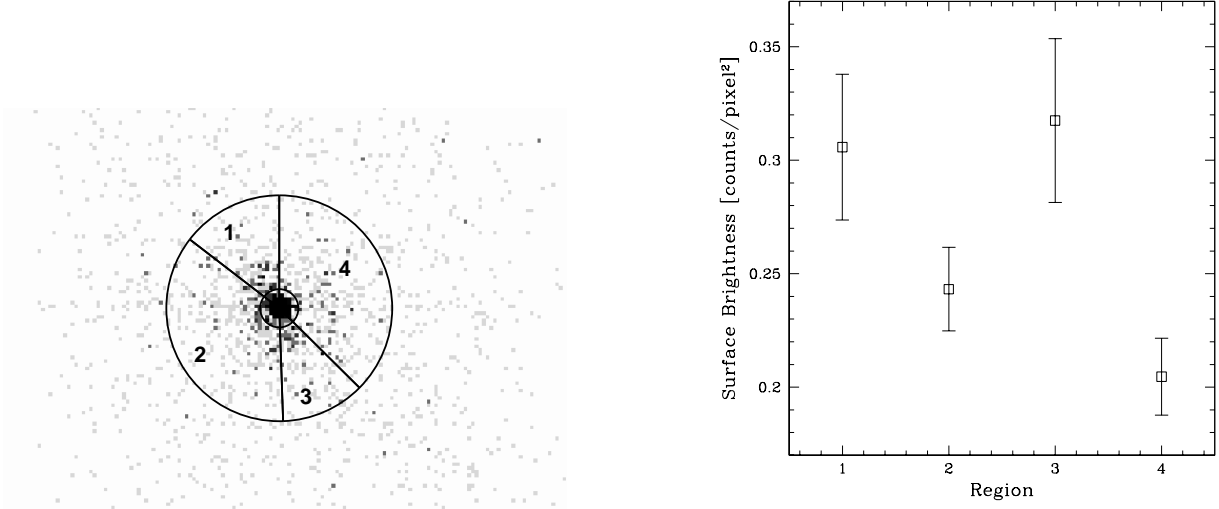


FIG. 7.— **Left:** Defined sector regions overlaid over an *Chandra* ACIS-S image of 3C 186. One pixel corresponds to  $0.492''$ . North is up and East is left. **Right:** Background subtracted surface brightness calculated for each sector in the left panel. The sector numbers are indicated on the bottom axis.

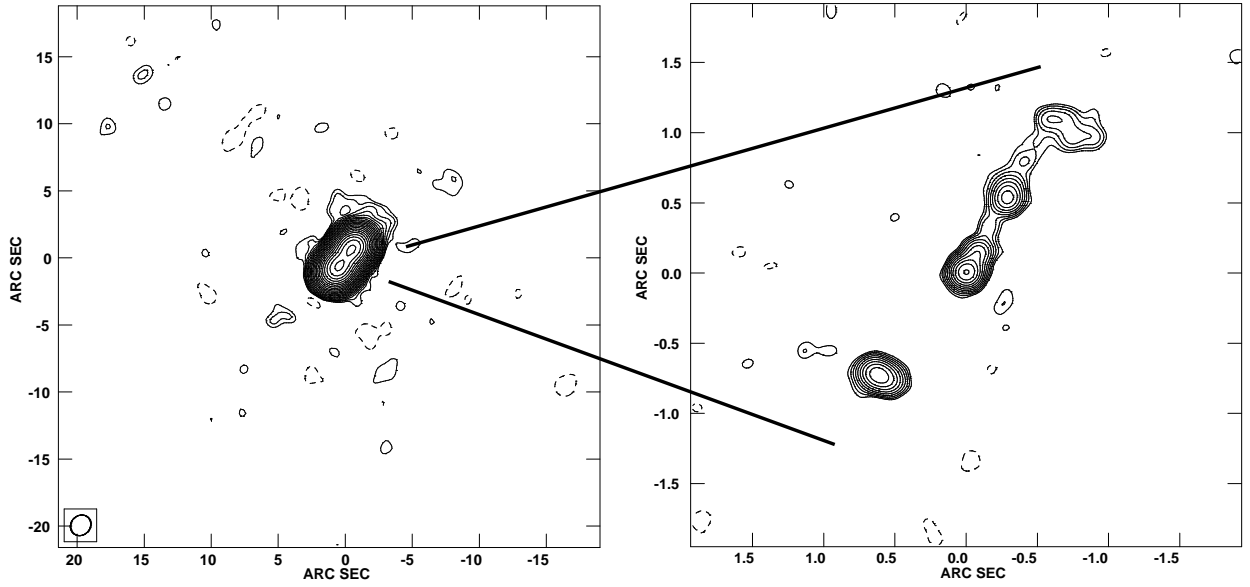


FIG. 8.— **Left:** VLA 1.5 GHz image of 3C 186 from reprocessing the A- and B-configuration archival datasets published in van Breugel et al. (1992). The restoring beam is  $1.62'' \times 1.44''$  at position angle  $-42.7$  degrees shown at bottom left. The image peak is  $565$  mJy/beam and contour levels begin at  $0.5$  mJy/beam ( $2\sigma$ ) and increase by factors of  $\sqrt{2}$ . Some extended radio emission is apparent, though not at the angular scale of the observed extended X-rays. North is up East is left. **Right:** High resolution ( $0.15''$ ) VLA 15 GHz image of 3C 186 showing the core-jet morphology of the source. The image peak is  $21.6$  mJy/beam, and contours begin at  $0.65$  mJy/beam increasing by factors of  $\sqrt{2}$ .

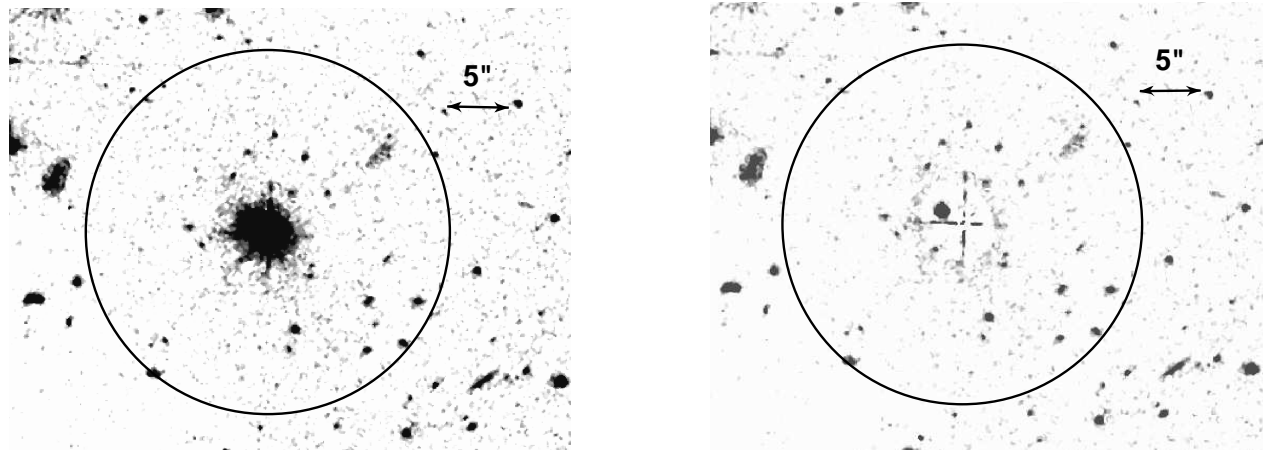


FIG. 9.— **Left:** HST image of the field. The  $15''$  radius circle highlights the region of the diffuse X-ray emission. North is up East is left. **Right:** The host galaxy contribution subtracted from the central image. The ring of diffuse emission between  $2-3''$  is an artifact of the imperfect galaxy subtraction. Also, the four diffraction spikes (the cross at the center) are apparent.

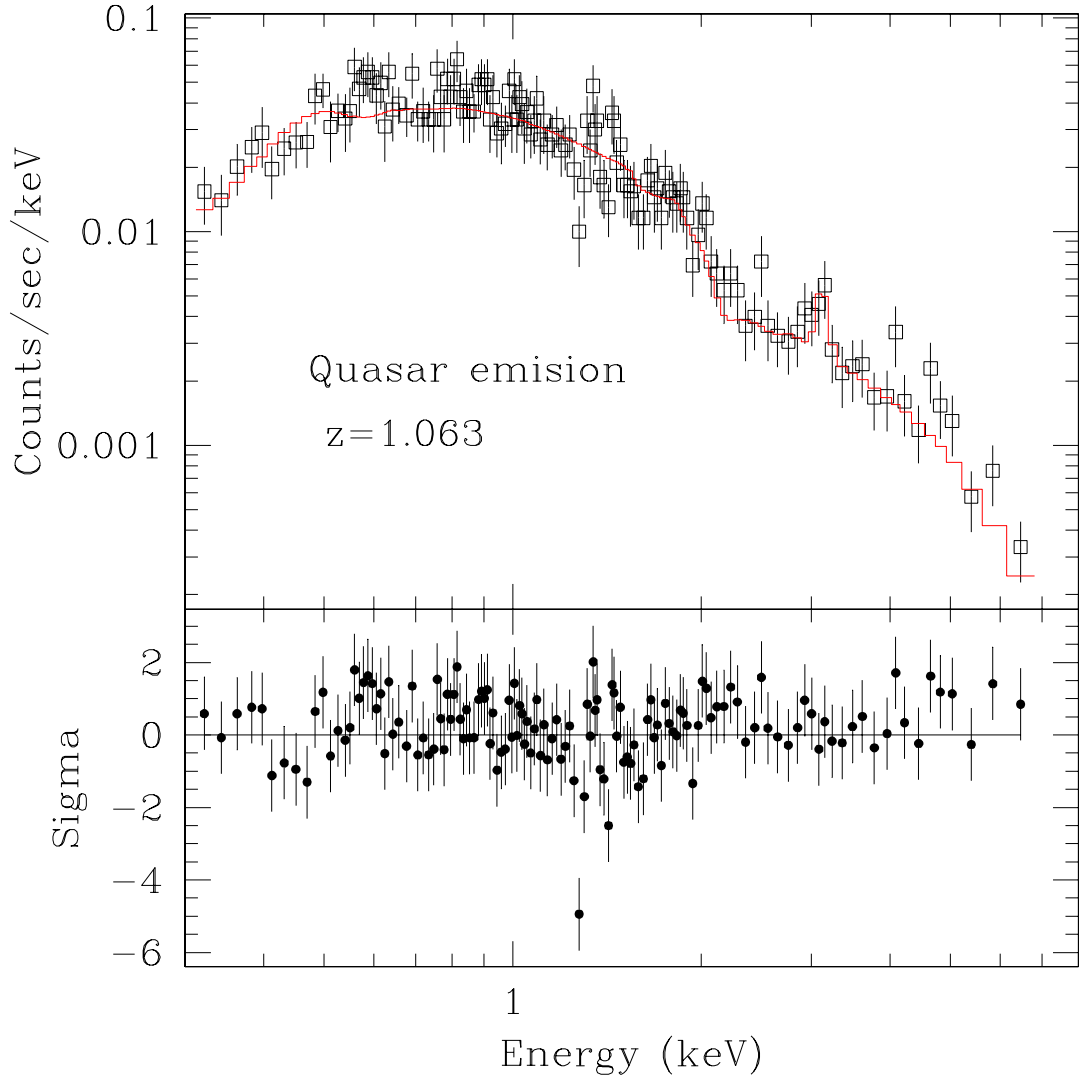


FIG. 10.— Upper panel shows the ACIS-S spectrum of the  $z=1.063$  quasar Q0740+380 (empty squares) over-plotted with the best-fit power law plus Gaussian line model at  $E_{obs} = 3.07^{+0.06}_{-0.11}$  keV (a solid line). The bottom panel shows the difference between model and the data in units of sigma. The scatter between 1 keV and 2 keV is due to calibration uncertainties.

This figure "f2.gif" is available in "gif" format from:

<http://arxiv.org/ps/astro-ph/0506394v1>

This figure "f3a.gif" is available in "gif" format from:

<http://arxiv.org/ps/astro-ph/0506394v1>

This figure "f3b.gif" is available in "gif" format from:

<http://arxiv.org/ps/astro-ph/0506394v1>